Magnetic Nanoparticles

DOI: 10.1002/anie.200805149

Critical Enhancements of MRI Contrast and Hyperthermic Effects by Dopant-Controlled Magnetic Nanoparticles**

*Jung-tak Jang, Hyunsoo Nah, Jae-Hyun Lee, Seung Ho Moon, Min Gyu Kim, and Jinwoo Cheon**

Magnetic characteristics are crucial for the successful performances of magnetic nanoparticles in biomedical applications such as magnetic resonance imaging (MRI), drug delivery, cellular signaling, and hyperthermia.[1–4] Therefore, the development of new types of nanoparticles is particularly important. In this regard, a metal dopant substitution strategy of metal ferrite nanoparticles has been pursued to achieve high and tunable nanomagnetism.[5] In the case of Zn^{2+} doping, however, the use of nonequilibrium reactions has typically resulted in nonstoichiometric or metastable states in which Zn^{2+} ions are disordered between T_d and O_h sites.[6–8] A recent report of successful Zn^{2+} doping includes the use of diethyl zinc (Et_2Zn) as a new Zn^{2+} ion source;[9] however, because of the highly unstable and pyrophoric nature of the precursor, such a synthetic protocol for nanoparticles is still far from ideal for the achievement of large-scale reproducibility and precise dopant controls. In this study, we have overcome a number of previous challenges; not only is size monodispersity with a large-scale (ca. 10 g) synthesis achieved, the proper positioning of Zn^{2+} dopants in T_d sites in metal ferrite nanoparticles is also demonstrated, which ultimately leads to successful magnetism tuning. Our obtained nanoparticles exhibit an extremely high magnetization value (175 emu g^{-1}) and provide the largest MRI contrast effects ($r2 = 860$ mM^{-1} s^{-1}) among the contrast agents reported to date. They have an eight- to fourteenfold increase in MRI contrast and a fourfold enhancement in hyperthermic effects compared to conventional iron oxide nanoparticles.

For decades, iron oxide (Fe_3O_4) nanoparticles have served as the model material in the biomedical research field associated with magnetism.[10] However, considering that the effects of magnetic nanoparticles for biomedical applications are strongly dependent on their magnetic characteristics, it is important to devise nanoparticles with high and tunable magnetism, especially saturation magnetization (M_s) values, while maintaining high size monodispersity. For example, nanoparticles with tunable magnetism, such as manganese-doped metal ferrite and FeCo nanoparticles, have enhanced MRI contrast effects that are significantly superior to that of conventional iron oxide nanoparticles.[5a,11] This enhancement is significant for clinical purposes as the nanoparticle probe dosage level can be progressively lowered when using probes that have improved contrast enhancement effects. In the first part of this study, we present a large-scale, simple, and reliable synthetic protocol to achieve Zn^{2+} doping controlled metal ferrite nanoparticles. A one-pot thermal decomposition method was used, which involved a metal chloride (MCl_2, $M = Zn^{2+}$, Mn^{2+}, and Fe^{2+}) and iron tris-2,4-pentadionate ($[Fe(acac)_3]$) in the presence of oleic acid, oleylamine, and octyl ether.[12] The Zn^{2+} doping level, a key parameter, was carefully controlled by varying the initial molar ratio of the metal chloride precursors. As shown in Figure 1 a–c, a series of 15 nm sized Zn^{2+} doped nanoparticles of $(Zn_xMn_{1-x})Fe_2O_4$ and $(Zn_xFe_{1-x})Fe_2O_4$ ($x = 0$, 0.1, 0.2, 0.3, 0.4, and 0.8) with single crystallinity and size monodispersity ($\sigma < 5\%$) were

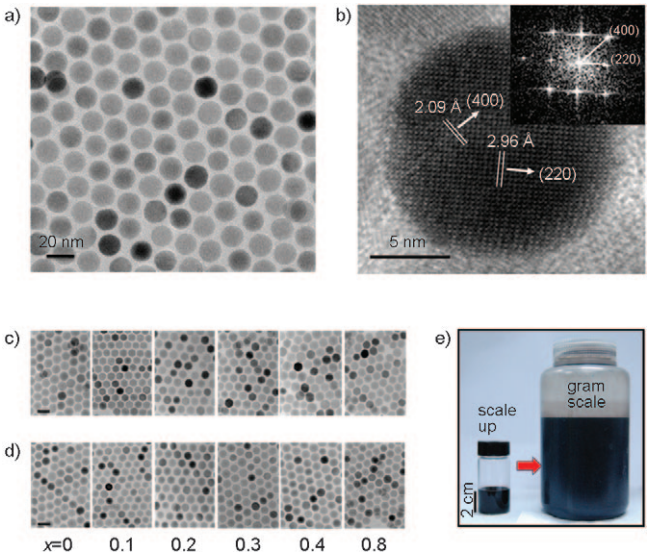

Figure 1. a) TEM image of 15 nm $(Zn_{0.4}Fe_{0.6})Fe_2O_4$ nanoparticles. b) High-resolution TEM image of 15 nm $(Zn_{0.4}Fe_{0.6})Fe_2O_4$ nanoparticles. The inset shows the FFT pattern. c, d) TEM images of 15 nm $(Zn_xMn_{1-x})Fe_2O_4$ (c) and $(Zn_xFe_{1-x})Fe_2O_4$ (d) nanoparticles (scale bar: 20 nm). e) Photograph showing that the synthesis of 15 nm $(Zn_{0.4}Fe_{0.6})Fe_2O_4$ nanoparticles can be scaled up to ca. 10 g.

[*] J.-t. Jang, H. Nah, J.-H. Lee, S. H. Moon, Prof. J. Cheon
Department of Chemistry, Yonsei University
Seoul 120-749 (Korea)
Fax: (+82) 2-364-7050
E-mail: jcheon@yonsei.ac.kr
Dr. M. G. Kim
Pohang Accelerator Laboratory (PAL)
Pohang 790-784 (Korea)

[**] We thank Prof. H. Ju and J. C. Moon for magnetic property measurements, and Dr. Y.-w. Jun and Dr. J.-w. Seo for helpful discussions. We thank J.-G Kim and Y.-J. Kim for TEM analyses (JEM-ARM1300S). This work was supported in part by the National Research Laboratory (R0A-2006-000-10255-0), 2nd stage BK21, AFOSR–AOARD (FA4869-08-1-4016), and the NCI Center for Cancer Nanotechnology Excellence (CCNE).

Supporting information for this article is available on the WWW under http://dx.doi.org/10.1002/anie.200805149.

successfully obtained. High-resolution transmission electron microscopy (TEM) analysis, its associated fast Fourier transformation (FFT) pattern (Figure 1d), and X-ray diffraction (XRD; see Figure S1 in the Supporting Information) indicate that the nanoparticles have high-quality crystallinity. Although typical syntheses were carried out to produce tens of milligrams of nanoparticles, the reaction was easily scaled up to the gram scale (ca. 10 g) in a one-pot reaction without sacrificing the quality of the nanoparticles (Figure 1e). The Zn^{2+} doping level was estimated by using energy dispersive X-ray spectroscopy (EDS) and inductively coupled plasma atomic emission spectroscopy (ICP-AES; see Figure S2 in the Supporting Information).

Additionally, it is important to confirm that the dopant Zn^{2+} ions mainly occupy T_d sites of the spinel matrix by using extended X-ray absorption fine structure (EXAFS) analysis to examine the Zn and Fe *K*-edges (Figure 2a). Fourier-transformed (FT) Fe *K*-edge k^3-weighted EXAFS spectra of $(Zn_xFe_{1-x})Fe_2O_4$ nanoparticles exhibit the characteristic FT peak features of a spinel structure. For the partially substituted Zn^{2+} ions, the FT peak at 3.1 Å in the Zn *K*-edge EXAFS spectra originates from central Zn^{2+} ions in T_d holes. The FT peak intensity gradually increases as the Zn^{2+} doping level of $(Zn_xFe_{1-x})Fe_2O_4$ nanoparticles increases from $x=0.1$ to 0.2, 0.3, and 0.4 (Figure 2a, red solid line). In contrast, the peak at 2.6 Å, which is due to the Zn^{2+} ions in O_h sites, is almost negligible (Figure 2a, black dotted line). Therefore, we conclude that the Zn^{2+} ions mainly reside in T_d sites rather than O_h sites.[13] Similarly, for $(Zn_xMn_{1-x})Fe_2O_4$ nanoparticles, the Zn^{2+} ion occupation in T_d sites is also confirmed by EXAFS analysis (see Figure S3 in the Supporting Information).

The magnetism of the Zn^{2+} doped metal ferrite nanoparticles was measured using a superconducting quantum interference device (SQUID) at 300 K (Figure 2e). The M_s value gradually increases as the Zn^{2+} doping level of $(Zn_xMn_{1-x})Fe_2O_4$ nanoparticle increased from $x=0$ to 0.1, 0.2, 0.3, and 0.4, with M_s values of 125, 140, 154, 166, and 175 emu g^{-1} (Zn + Mn + Fe), respectively. The M_s value reaches its maximum at $x=0.4$ but diminishes to 137 emu g^{-1} at $x=0.8$ (Figure 2e, red line). In a similar fashion to $(Zn_xFe_{1-x})Fe_2O_4$ nanoparticles, the M_s value changes from 114 to 126, 140, 152, 161, and 115 emu g^{-1} (Zn + Fe) for $x=0$ to 0.1, 0.2, 0.3, 0.4, and 0.8, respectively (Figure 2e, black line). In both cases, the M_s value reaches its maximum of 175 emu g^{-1} (Zn + Mn + Fe) and 161 emu g^{-1} (Zn + Fe) at $x=0.4$, which far exceeds the value of 127 emu g^{-1} (Fe) observed for undoped bulk iron oxide (Fe_3O_4), and are the highest values observed among the various metal ferrite nanoparticles reported to date.[14]

The magnetism tuning of nanoparticles is successful since the change of antiferromagnetic coupling interactions between T_d and O_h sites can be modulated by using Zn^{2+} dopants.[15] For instance, when Zn^{2+} ions are added to the unit cell of a spinel structure ($x<0.4$), they occupy T_d sites (Figure 2c). This phenomenon induces the partial removal of antiferromagnetic coupling interactions between Fe^{3+} ions in the T_d and O_h sites.[16] Incremental changes in the M_s value are therefore clearly observed (Figure 2b–d). However, at very high Zn^{2+} ion levels, antiferromagnetic coupling interactions between Fe^{3+} ions in each O_h site are dominant and the net magnetization moment decreases. In fact, the theoretical magnetization value of pure $ZnFe_2O_4$ ($x=1$) is calculated to be zero.[17]

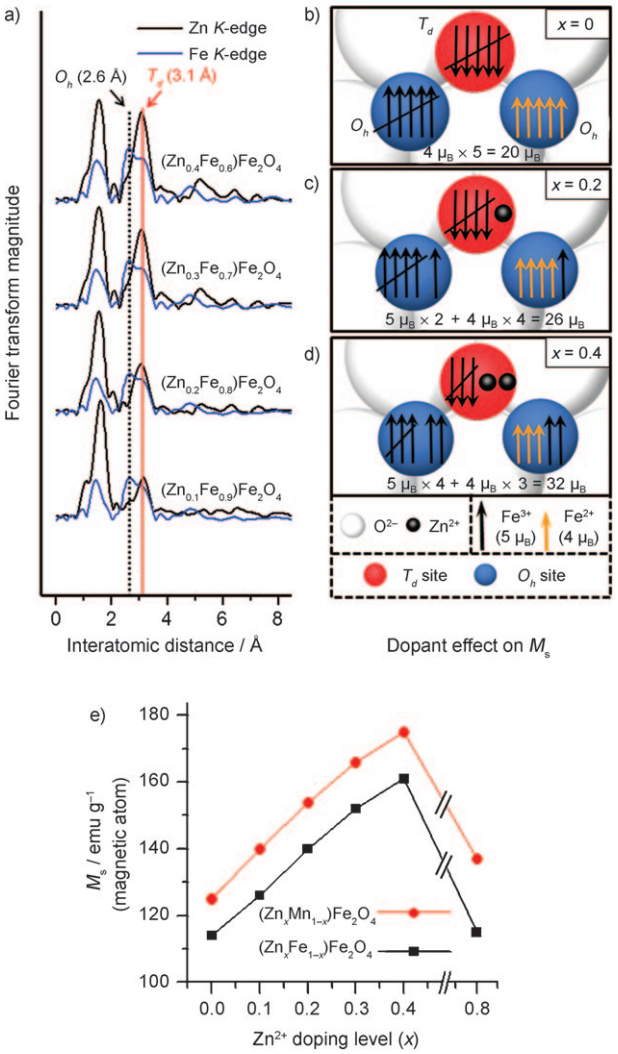

Figure 2. a) Zn *K* edge EXAFS spectra of $(Zn_xFe_{1-x})Fe_2O_4$ nanoparticles ($x=0.1$, 0.2, 0.3, and 0.4). The intensity of the peak at 3.1 Å (red line) gradually becomes stronger as the Zn^{2+} doping level is increased, which indicates that the amounts of Zn^{2+} ions in T_d sites progressively increase. b) Undoped, c) Zn^{2+} doped ($x=0.2$), and d) Zn^{2+} doped ($x=0.4$) magnetic spin alignment diagrams in spinel-structured $(Zn_xFe_{1-x})Fe_2O_4$ nanoparticles under an applied magnetic field. e) Graphs of M_s versus Zn^{2+} doping level $(Zn_xM_{1-x})Fe_2O_4$ (M = Mn^{2+}, Fe^{2+}) nanoparticles (red line: $(Zn_xMn_{1-x})Fe_2O_4$, black line: $(Zn_xFe_{1-x})Fe_2O_4$).

In MRI, the contrast enhancement effects are directly related to the M_s value of the nanoparticles. Specifically, spin–spin relaxivity ($R2=1/T2$) represents the degree of *T*2-weighted MRI contrast effect where the *R*2 value is roughly proportional to the square of the M_s value.[18] The Zn^{2+} dopant effects of metal ferrite nanoparticles on the MRI contrast enhancements were measured at 4.5 T and compared with the effects of conventional iron oxide nanoparticles (Feridex and cross-linked iron oxide (CLIO)) with the same

concentration and MRI sequence (Figure 3a–c). The relaxivity coefficient ($r2$), which is obtained as the gradient of the plot of $R2$ versus the molarity of magnetic atoms, increases as the Zn^{2+} doping level of $(Zn_xMn_{1-x})Fe_2O_4$ nanoparticles

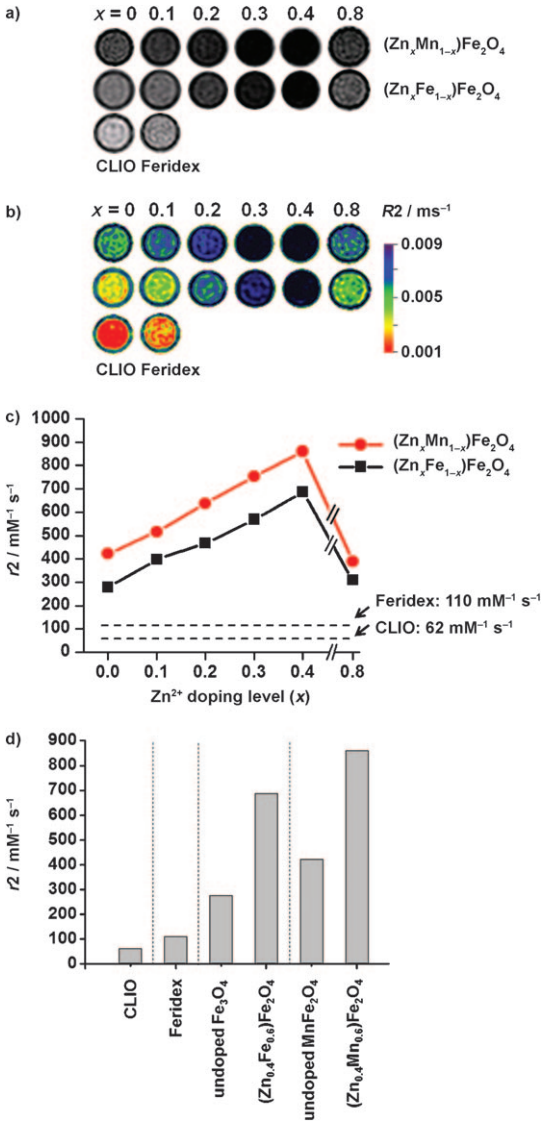

Figure 3. MR contrast effects of $(Zn_xM_{1-x})Fe_2O_4$ ($M = Mn^{2+}$, Fe^{2+}) nanoparticles upon changes in the Zn^{2+} doping level. a) $T2$-weighted MR images of $(Zn_xM_{1-x})Fe_2O_4$ ($M = Mn^{2+}$, Fe^{2+}) nanoparticles, Feridex, and CLIO and b) their color-coded images, where red indicates low $R2$ and violet indicates high $R2$ values. c) Graphs of $r2$ versus Zn^{2+} doped $(Zn_xM_{1-x})Fe_2O_4$ ($M = Mn^{2+}$, Fe^{2+}) nanoparticles at 4.5 T. d) Comparison of $r2$ values of nanoparticles, showing that Zn^{2+} doped nanoparticles have significantly enhanced MRI contrast effects compared to conventional iron oxide nanoparticles.

increases from $x = 0$ to 0.1, 0.2, 0.3, and 0.4 with values of 422, 516, 637, 754, and 860 $mM^{-1}s^{-1}$, respectively. The $r2$ value reaches its maximum at $x = 0.4$ but decreases to 388 $mM^{-1}s^{-1}$ at $x = 0.8$ (Figure 3c, red line). Similarly, for $(Zn_xFe_{1-x})Fe_2O_4$ nanoparticles, the $r2$ value changes from 276 to 397, 466, 568, 687, and 307 $mM^{-1}s^{-1}$ for $x = 0$ to 0.1, 0.2, 0.3, 0.4, and 0.8, respectively (Figure 3c, black line). The $r2$ value of CLIO is 62 $mM^{-1}s^{-1}$ and Feridex is 110 $mM^{-1}s^{-1}$ (Figure 3c, dashed lines). Based on the $r2$ values, the 15 nm sized $(Zn_{0.4}Mn_{0.6})Fe_2O_4$ nanoparticles have MRI contrast effects of 860 $mM^{-1}s^{-1}$ that are 13.8 and 7.8 times larger than those of CLIO and Feridex, respectively. Also, these $(Zn_{0.4}Fe_{0.6})Fe_2O_4$ and $(Zn_{0.4}Mn_{0.6})Fe_2O_4$ nanoparticles have superior MRI contrast effects that are 2.5 and 2 times larger than those of undoped Fe_3O_4 (276 $mM^{-1}s^{-1}$) and $MnFe_2O_4$ (422 $mM^{-1}s^{-1}$) nanoparticles, respectively (Figure 3d).

The high M_s value of the nanoparticles can also be used to achieve magnetically induced heat generation for the thermal treatment of cancer and other diseases.[19] Enhancement of SLP (specific loss power), the standard criterion for hyperthermia effects (defined as the thermal power dissipation divided by the mass of the magnetic material and the heat capacity of solution), is important in order to obtain high efficacy with smaller dose levels in biomedical applications.[20] The SLP values are highly dependent on magnetic relaxation processes and are roughly proportional to the M_s value and the magnetocrystalline anisotropy constant (K), and are inversely proportional to the size distribution of the nanoparticles (σ).[21] Our 15 nm sized $(Zn_{0.4}Mn_{0.6})Fe_2O_4$ nanoparticles with a high M_s value of 175 emu g^{-1} ($Zn + Mn + Fe$), monodispersity ($\sigma < 5\%$), and increased anisotropy are therefore ideal candidates for hyperthermic studies. The SLP value of $(Zn_{0.4}Mn_{0.6})Fe_2O_4$ nanoparticles is 432 W g^{-1}, which is four times larger than that of Feridex (115 W g^{-1}) when measured under identical conditions (Figure 4a). Further in vitro hyperthermic cancer cell treatment tests were performed. As shown in Figure 4b, most (84.4%) HeLa cells treated with $(Zn_{0.4}Mn_{0.6})Fe_2O_4$ nanoparticles died after 10 minutes of alternating current (AC) magnetic field appli-

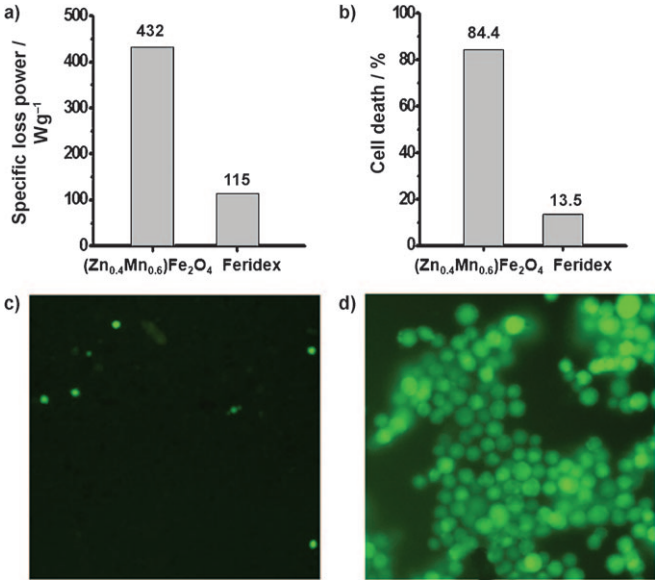

Figure 4. a) SLP values for $(Zn_{0.4}Mn_{0.6})Fe_2O_4$ and Feridex in a 500 kHz AC magnetic field with an amplitude of 3.7 kA m^{-1}. b) Percentage of HeLa cells killed after treatment with $(Zn_{0.4}Mn_{0.6})Fe_2O_4$ nanoparticles or Feridex and the subsequent application of an AC magnetic field for 10 min. Fluorescence microscopy images of AC magnetic field applied HeLa cells treated with c) $(Zn_{0.4}Mn_{0.6})Fe_2O_4$ nanoparticles and d) Feridex, stained with calcein indicating live cells as green fluorescence.

cation, whereas only 13.5% of cells died when treated with Feridex. After AC magnetic field application, fluorescence microscope images in which live cells were stained with calcein, which emits green fluorescence, show very weak fluorescence for the cells treated with $(Zn_{0.4}Mn_{0.6})Fe_2O_4$ nanoparticles, whereas intense green fluorescence is observed for those treated with Feridex (Figure 4c,d). Additionally, our preliminary in vitro study indicates that these Zn^{2+} doped nanoparticles are nontoxic to healthy cells (see Figure S7 in the Supporting Information).

We have successfully demonstrated that the high magnetism of metal ferrite nanoparticles can be very effectively modulated and achieved by Zn^{2+} dopant control. The nanoparticles act as MR contrast and hyperthermia agents, which have *r*2 values that are eight to fourteen times greater for MRI and SLP values that are four times greater for hyperthermia cancer cell treatments than conventional nanoparticle agents. In addition, these nanoparticles are nontoxic. Such high-performance magnetic nanoparticles fabricated by using this magnetism engineering concept could play a significant role in the improvement of current diagnostics, therapeutics, and other biomedical studies such as cell actuation.

Experimental Section

Materials and instruments: All chemicals were purchased from Aldrich. Zinc(II) chloride, manganese(II) chloride, iron(II) chloride, and iron(III) tri-2,4-pentadionate were used as received. Oleic acid and oleylamine were purified by distillation under an argon atmosphere. Feridex was obtained from TAEJOON Pharmaceutical Co. Transmission electron microscopy (TEM) and high-resolution TEM analyses were performed on JEOL-2100 and JEM-ARM 1300S instruments. Elemental analysis was carried out by using inductively coupled plasma atomic emission spectroscopy (OPTIMA 4300DV, PerkinElmer, USA) and energy dispersive X-ray spectroscopy (EDS; INCA, Oxford Instruments). X-ray powder diffraction studies were conducted using a Rigaku D/MAX-RB diffractometer equipped with a graphite-monochromated $Cu_{K\alpha}$ radiation source (40 kV, 120 mA). Magnetic properties were measured with a superconducting quantum interference device (SQUID) magnetometer (Quantum Design MPMS-7).

15 nm $(Zn_xMn_{1-x})Fe_2O_4$ and $(Zn_xFe_{1-x})Fe_2O_4$ ($x = 0$, 0.1, 0.2, 0.3, 0.4, and 0.8) nanoparticles were prepared following a slightly modified procedure.[5a,11] A typical small-scale synthesis to produce $(Zn_{0.4}Mn_{0.6})Fe_2O_4$ nanoparticles is as follows: $ZnCl_2$ (0.03 g), $MnCl_2$ (0.04 g), and $[Fe(acac)_3]$ (0.353 g) were placed in a 50 mL three-neck round-bottom flask in the presence of surfactants (oleic acid and oleylamine) in octyl ether. The reaction mixture was heated at 300 °C for 1 h and, after removing the heating source, the reaction products were cooled to room temperature. Upon addition of ethanol, a black powder precipitated and was isolated by centrifugation. The isolated nanoparticles were dispersed in a solvent such as toluene. The typical yield of nanoparticles was 40 mg. For large-scale synthesis, the same procedures were utilized in which the amounts of reagents used were $ZnCl_2$ (3.6 g), $MnCl_2$ (4.8 g), and $[Fe(acac)_3]$ (42.4 g) and the yield of obtained nanoparticles was 9.8 g. $(Zn_{0.4}Fe_{0.6})Fe_2O_4$ nanoparticles were obtained by using $FeCl_2$ instead of $MnCl_2$ under identical conditions. In order to control the Zn^{2+} doping level, different amounts of Zn^{2+}/Mn^{2+} or Zn^{2+}/Fe^{2+} metal chloride precursors were used under identical conditions. $(Zn_{0.1}Mn_{0.9})Fe_2O_4$: $ZnCl_2$ (0.01 g) and $MnCl_2$ (0.06 g); $(Zn_{0.2}Mn_{0.8})Fe_2O_4$: $ZnCl_2$ (0.015 g) and $MnCl_2$ (0.05 g); $(Zn_{0.3}Mn_{0.7})Fe_2O_4$: $ZnCl_2$ (0.02 g) and $MnCl_2$ (0.045 g); $(Zn_{0.8}Mn_{0.2})Fe_2O_4$: $ZnCl_2$ (0.06 g) and $MnCl_2$(0.015 g). In the case of $(Zn_xFe_{1-x})Fe_2O_4$ nanoparticles, an equivalent amount of $FeCl_2$ was used instead of $MnCl_2$. The organic surfactants on the nanoparticle surface were removed and exchanged with 2,3-dimercaptosuccinic acid (DMSA) to make the nanoparticles completely dispersed in the aqueous medium.[22] Then these water-soluble nanoparticles were used for MR measurements and hyperthermic experiments.

SLP measurements and in vitro hyperthermia experimental methods: The sample of nanoparticles ($(Zn_{0.4}Mn_{0.6})Fe_2O_4$ or Feridex, 5 mg mL^{-1}) was placed inside a water-cooled copper coil which produced an alternating magnetic field in the frequency range of 500 kHz with an amplitude of up to 3.7 kA m^{-1}. The temperature was measured with a thermometer (TES-1307) placed in the center of the sample. In order to compare cell extinction effects, HeLa cells (1×106 cells), which were treated with $(Zn_{0.4}Mn_{0.6})Fe_2O_4$ nanoparticles and Feridex (0.5 mg mL^{-1}), respectively, were heated for 10 min.

MRI contrast effect measurement of Zn^{2+} doped metal ferrite nanoparticles: All MRI experiments were performed with a 4.7 T animal MRI instrument (Bruker, Germany) with a 72 mm volume coil at the Korea Basic Science Institute in Ochang. We measured the relaxivity coefficients ($r2$, mM^{-1} s^{-1}) of various $(Zn_xM_{1-x})Fe_2O_4$ nanoparticles ($x = 0$, 0.1, 0.2, 0.3, 0.4, and 0.8, M = Mn^{2+}, Fe^{2+}) by using the Carr–Purcell–Meiboom–Gill (CPMG) sequence at room temperature: TR(repetition time) = 5 s, 128 echoes with 7 ms even echo space, 2 acquisitions, in-plane pixel size = 547 μm × 547 μm, section thickness = 2 mm.

XAS measurements: Zn, Fe, and Mn *K*-edge X-ray absorption spectra were recorded on the BL7C1 beam line of the Pohang light source with a ring current of 130–190 mA at 2.5 GeV. A Si(111) double-crystal monochromator was employed to monochromatize the X-ray photon energy. The incident X-ray photon flux was monitored by N_2 gas-filled ionization. The EXAFS data from samples were collected in fluorescence mode. Higher-order harmonic contaminations were eliminated by detuning to reduce the incident X-ray intensity by approximately 30%. Energy calibration was simultaneously carried out for each measurement with Zn, Fe, and Mn metallic films placed in front of the third ion chamber.

Received: October 21, 2008
Published online: January 9, 2009

Keywords: imaging agents · magnetic properties · magnetism engineering · nanostructures · zinc

[1] a) E. Roduner, *Nanoscopic Materials: Size-Dependent Phenomena*, RSC, London, **2006**; b) S. Sun, *Adv. Mater.* **2006**, *18*, 393–403; c) Y.-w. Jun, J.-w. Seo, J. Cheon, *Acc. Chem. Res.* **2008**, *41*, 179–189; d) A.-H. Lu, E. L. Salabas, F. Schüth, *Angew. Chem.* **2007**, *119*, 1242–1266; *Angew. Chem. Int. Ed.* **2007**, *46*, 1222–1240; e) U. Jeong, X. Teng, Y. Wang, H. Yang, Y. Xia, *Adv. Mater.* **2007**, *19*, 33–60.

[2] a) J. W. M. Bulte, D. L. Kraitchman, *NMR Biomed.* **2004**, *17*, 484–499; b) D. L. J. Thorek, A. K. Chen, J. Czupryna, A. Tsourkas, *Ann. Biomed. Eng.* **2006**, *34*, 23–38; c) Y.-w. Jun, J.-H. Lee, J. Cheon, *Angew. Chem.* **2008**, *120*, 5200–5213; *Angew. Chem. Int. Ed.* **2008**, *47*, 5122–5135.

[3] a) J. Gao, L. Li, P.-L. Ho, G. C. Mak, H. Gu, B. Xu, *Adv. Mater.* **2006**, *18*, 3145–3148; b) T. Leakakos, C. Ji, G. Lawson, C. Peterson, S. Goodwin, *Cancer Chemother. Pharmacol.* **2003**, *51*, 445–450; c) P. Moroz, S. K. Jones, B. N. Gray, *Int. J. Hyperthermia* **2002**, *18*, 267–284.

[4] a) R. J. Mannix, S. Kumar, F. Cassiola, M. Montoya-Zavala, E. Feinstein, M. Prentiss, D. E. Ingber, *Nat. Nanotechnol.* **2008**, *3*, 36–40; b) J. Dobson, *Nat. Nanotechnol.* **2008**, *3*, 139–143.

[5] a) J.-H. Lee, Y.-M. Huh, Y.-w. Jun, J.-w. Seo, J.-t. Jang, H.-T. Song, S.-j. Kim, E.-J. Cho, H.-G. Yoon, J.-S. Suh, J. Cheon, *Nat. Med.* **2007**, *13*, 95–99; b) C. Liu, B. Zou, A. J. Rondinone, Z. J. Zhang, *J. Am. Chem. Soc.* **2000**, *122*, 6263–6267; c) R. A.

McCurrie, *Ferromagnetic Materials: Structure and Properties*, Academic Press, New York, **1994**; d) J. E. Thompson, *The Magnetic Properties of Materials*, Stonebridge Press, Bristol, **1968**.

[6] a) J. F. Hochepied, P. Bonville, M. P. Pileni, *J. Phys. Chem. B* **2000**, *104*, 905 – 912; b) J. F. Hochepied, M. P. Pileni, *J. Appl. Phys.* **2000**, *87*, 2472 – 2478; c) R. Arulmurugan, B. Jeyadevan, G. Vaidyanathan, S. Sendhilnathan, *J. Magn. Magn. Mater.* **2005**, *288*, 470 – 477.

[7] a) G. F. Goya, H. R. Rechenberg, M. Chen, W. B. Yelon, *J. Appl. Phys.* **2000**, *87*, 8005 – 8007; b) C. Rath, N. C. Mishra, S. Anand, R. P. Das, K. K. Sahu, C. Upadhyay, H. C. Verma, *Appl. Phys. Lett.* **2000**, *76*, 475 – 477; c) S. A. Oliver, V. G. Harris, H. H. Hamdeh, J. C. Ho, *Appl. Phys. Lett.* **2000**, *76*, 2761 – 2763.

[8] a) S. Nakashima, K. Fujita, K. Tanaka, K. Hirao, *J. Phys. Condens. Matter* **2005**, *17*, 137 – 149; b) K. Tanaka, S. Nakashima, K. Fujita, K. Hirao, *J. Appl. Phys.* **2006**, *99*, 106103.

[9] C. Bárcena, A. K. Sra, G. S. Chaubey, C. Khemtong, J. P. Liu, J. Gao, *Chem. Commun.* **2008**, 2224 – 2226.

[10] a) M. Kettering, J. Winter, M. Zeisberger, S. B. Streck, H. Oehring, C. Bergemann, C. Alexxiou, R. Hergt, K. J. Halbhuber, W. A. Kaiser, I. Hilger, *Nanotechnology* **2007**, *18*, 175101; b) R. Hergt, R. Hiergeist, M. Zeisberger, G. Glockl, W. Weitschies, L. P. Ramirez, I. Hilger, W. A. Kaiser, *J. Magn. Magn. Mater.* **2004**, *280*, 358 – 368; c) R. Weissleder, A. Moore, U. Mahmood. E. Bhorade, H. Benveniste, E. A. Chiocca, J. P. Basilion, *Nat. Med.* **2000**, *6*, 351 – 354.

[11] a) W. S. Seo, J. H. Lee, X. Sun, Y. Suzuki, D. Mann, Z. Liu, M. Terashima, P. C. Yang, M. V. Mcconnell, D. G. Nishimura, H. Dai, *Nat. Mater.* **2006**, *5*, 971 – 976; b) G. S. Chaubey, C. Barcena, N. Poudyal, C. Rong, J. Gao, S. Sun, J. P. Liu, *J. Am. Chem. Soc.* **2007**, *129*, 7214 – 7215.

[12] a) S. Sun, C. B. Murray, D. Weller, L. Folks, A. Moser, *Science* **2000**, *287*, 1989 – 1992; b) S. Sun, H. Zeng, D. B. Robinson, S. Raoux, P. M. Rice, S. X. Wang, G. Li, *J. Am. Chem. Soc.* **2004**, *126*, 273 – 279; c) J. Park, K. An, Y. Hwang, J.-G. Park, H.-J. Noh, J.-Y. Kim, J.-H. Park, N.-H. Hwang, T. Hyeon, *Nat. Mater.* **2004**, *3*, 891 – 895; d) N. R. Jana, Y. Chen, X. Peng, *Chem. Mater.* **2004**, *16*, 3931 – 3935.

[13] a) S. Nakashima, K. Fujita, K. Tanaka, K. Hirao, T. Yamamoto, I. Tanaka, *Phys. Rev. B* **2007**, *75*, 174443; b) S. J. Stewart, S. J. Figueroa, J. M. R. Lopez, S. G. Marchetti, J. F. Bengoa, R. J. Prado, F. G. Requejo, *Phys. Rev. B* **2007**, *75*, 073408.

[14] R. M. Cornel, U. Schwertmann, *The Iron Oxides*, Wiley-VCH, Weinheim, **2000**.

[15] B. D. Cullity, *Introduction to Magnetic Materials*, Addison-Wesley, London, **1972**.

[16] P. G. Bercoff, H. R. Bertorello, *J. Magn. Magn. Mater.* **1997**, *169*, 314 – 322.

[17] A. Martin, M. K. Krause, I. Halevy, J. Gal, W. Schafer, G. Will, M. Hillberg, R. Wappling, *Phys. Rev. B* **1996**, *53*, 9143 – 9152.

[18] S. H. Koenig, K. E. Keller, *Magn. Reson. Med.* **1995**, *34*, 227 – 233.

[19] S. Mornet, S. Vesseur, F. Grasset, E. Duguet, *J. Mater. Chem.* **2004**, *14*, 2161 – 2175.

[20] J.-P. Fortin, C. Wilhelm, J. Servais, C. Menager, J.-C. Bacri, F. Gazeau, *J. Am. Chem. Soc.* **2007**, *129*, 2628 – 2635.

[21] R. E. Rosensweig, *J. Magn. Magn. Mater.* **2002**, *252*, 370 – 374.

[22] Y.-w. Jun, Y.-M. Huh, J.-s. Choi, J.-H. Lee, H.-T. Song, S. Kim, S. Kim, S. Yoon, K.-S. Kim, J.-S. Shin, J.-S. Suh, J. Cheon, *J. Am. Chem. Soc.* **2005**, *127*, 5732 – 5733.

